Li et al. Heritage Science (2023) 11:253
https://doi.org/10.1186/s40494-023-01085-1

Heritage Science

RESEARCH Open Access

Study on the structural stability of the blistering of the Vajrasana pagoda in Miaozhan Temple, Kunming, Yunnan, China

Bo Li[1], Yao Zhang[2,3], Xun Bao[4*], Yu Wang[1], Ying Zhang[5], Deshan Cui[4] and Hong Guo[3*]

Abstract

The Vajrasana pagoda is the only stone overturned-bowl pagoda among the 12 existing Vajrasana pagodas built during the Ming Dynasty in the Guandu District, Kunming City, Yunnan Province, China. The location of the Vajrasana pagoda is in an earthquake-active zone with high rainfall. The small towers on the upper side were damaged by an earthquake in 1696 AD. All the stone statues representing religious figures have blistered and may peel further due to external factors, such as sunshine and rainfall. To assess the structural stability of the blistering, we employed 3D laser scanning to record the building's geometry over time. Subsequently, X-ray diffraction, thin section identification, and uniaxial compressive strength tests were conducted on the pagoda stone to reveal physical–mechanical properties. Finally, a finite element model was constructed to analyze stress and displacement in various scenarios. The results revealed: (1) Blistering on the pagoda stone is secure under self-gravity and heavy rainfall. (2) In an earthquake, the upper blistering near the junction of two sides may break. (3) A 3D color deviation model of blistering over 8 months showed peeling and bursting within the finite element simulation's predicted range. This research offers a fresh approach to stone tower preservation, shifting from reactive measures to proactive prevention and prediction. These methods and concepts hold relevance for stone towers in similar high-rainfall and earthquake-prone regions.

Keywords Vajrasana pagoda in Miaozhan Temple, Finite element analysis, Structural stability, Heavy rainfall, Earthquake, Three-dimensional laser scanning

Introduction

Most cultural heritage sites suffer damage due to material deterioration, affecting their structural stability and appearance. Natural disasters, such as earthquakes and severe storms [1], pose significant threats to their preservation. Between 1998 and 2017, 7.8% of global disasters were earthquake-related, with an additional 28.2% caused by severe storms. During March 2022, there were 1154 recorded world cultural heritage sites, including 39 cultural and natural heritage sites, of which 52 were endangered (about 4.5% of the total). Deformation is a primary challenge for architectural heritage sites, given their large size, weight, complex structures, and exposure to severe weathering. Monitoring deformation traditionally relied on manual inspections [2, 3] and instruments [4, 5] but

*Correspondence:
Xun Bao
990413@cug.edu.cn
Hong Guo
Guohong@ustb.edu.cn
[1] Beijing Guowenyan Conservation and Development of Cultural Heritage Co., Ltd, Beijing 100192, China
[2] School of Archaeology and Museology, Peking University, Beijing 100871, China
[3] Institute of Cultural Heritage and History of Science & Technology, University of Science and Technology Beijing, Beijing 100083, China
[4] Faculty of Engineering, China University of Geosciences, Wuhan 430074, Hubei, China
[5] Kunming Guandu District Museum, Kunming 650200, Yunnan, China

suffered from subjectivity and incomplete data, limiting accurate prediction and prevention. Surface features like statues and inscriptions convey cultural significance, and their loss devalues relics. Existing methods mostly focus on overall deformation, with little attention to local areas. To address these limitations, we employ the finite element method for precise local deformation estimation and propose innovative preventive protection strategies.

The Finite Element Method (FEM) is a versatile numerical simulation technique used for analyzing stress, strain, displacement, and other factors affecting an object under various environmental conditions. It reveals the object's deformation and damage patterns. FEM has been applied in structural analysis for buildings [6–8], pavilions [9], temples [10], grottoes [11], tombs [12], and wooden samples [13]. Model accuracy significantly influences the precision of finite element analysis results. In cultural relic preservation, large structures often employ surveying data to create finite element models for overall stress and strain analysis. However, for objects with irregular shapes and complex topology, traditional modeling is time-consuming and lacks accuracy, especially for local stress analysis. Advancements in 3D laser scanning, computer visualization, image processing, digitization, and virtual reality have ushered cultural relic preservation into the information age, allowing the acquisition of high-precision geometric data. Using these high-precision models for finite element analysis enables detailed artifact examination. FEM can handle nonlinearity, heterogeneity, multiple unit modes, material models, and analysis processes. ABAQUS, a powerful and versatile finite element software, was used in this study to examine nonlinear, elastic–plastic properties, shear expansion, and anisotropy in the complex relationship between stress and strain in rock and soil samples.

Cultural relic preservation has transitioned into the digital age, with digital protection becoming a key research focus [14, 15]. This method is unaffected by weather, lighting, color, and provides accurate high-resolution 3D digital records used for documentation, archiving, conservation, restoration, heritage monitoring, replication, display, and visualization [16, 17]. Scholars have identified and measured deterioration, such as cracks [18], physical and chemical weathering [19], and deformation [20, 21], in point cloud [22] and 3D color models [23], meeting specific conservation needs [24].

The Vajrasana Pagoda in Miaozhan Temple is located in a seismically active zone with a concentrated monsoon climate characterized by heavy rainfall. The small towers of the pagoda were damaged in a 1696 earthquake, and the structure still suffers from seepage, skewing, and settlement due to strata, preservation environment, and cultural factors. Stone statues on the main tower have developed blisters, a common deterioration issue in stone relics, often affecting the surface layer's artistic and cultural significance. Preventing further blistering is crucial.

By addressing settlement and concrete backfilling, the overall stability of the Vajrasana pagoda has improved. The main challenge now is to assess blistering stability and predict potential peeling areas without causing damage. Extensive research on the Vajrasana pagoda's structural stability included a strata survey, laser scanning, material property analysis, and mineral composition detection of blistering materials. Nonlinear static analyses in ABAQUS software were conducted, simulating self-gravity, heavy rainfall, and earthquakes to evaluate stress and strain at the pagoda's critical points, ensuring its stability. This research forms a strong foundation for preserving, restoring, maintaining, and monitoring cultural heritage sites (Fig. 1).

Environment characterization of the Vajrasana pagoda

Introduction to the Vajrasana Pagoda

The Vajrasana Pagoda holds significant religious and cultural importance in China, serving as a center for cultural exchanges and ethnic integration. In the dissemination of religion, pagodas, murals, and sculptures prove more impactful than scriptures and documents, effectively conveying their message. Introduced during the Eastern Han Dynasty, the Vajrasana Pagoda style from India became prominent in China during the Northern Dynasty. Originating in ancient India in the third century BC, it evolved into the five-tower Buddha Gaya Pagoda during the sixth century AD, under the Gupta period [25].

China houses 12 Vajrasana Pagodas, with only the one at Miaozhan Temple constructed from stone, while the others combine bricks and stones [26]. Situated in Guandu District, Kunming City, Yunnan Province, the Vajrasana Pagoda in Miaozhan Temple was built in 1458 AD during the Ming Dynasty (Fig. 2a, b). This pagoda, characterized by its overturned-bowl structure, consists of one base and five towers. The base follows the Xumi style and features nine square inscriptions on each side, with a central cross passage. The five towers, designed in the Lama Tower style, vary in height, with the main tower being the tallest. Carvings of mounts, ritual instruments symbolizing the Five Buddhas, and other statues adorn all sides of the main tower. The Miaozhan Temple's Vajrasana Pagoda stands at a total height of 17,156 mm, constructed from sandstone masonry. The base measures 10,520 mm in length and 4861 mm in height, the main tower is 5500 mm long and 12,295 mm high, and the small tower section is 1620 mm long and 4774 mm high.

As per the "Reconstruction of the Miaozhan Temple Pagoda" inscription, two small towers collapsed during

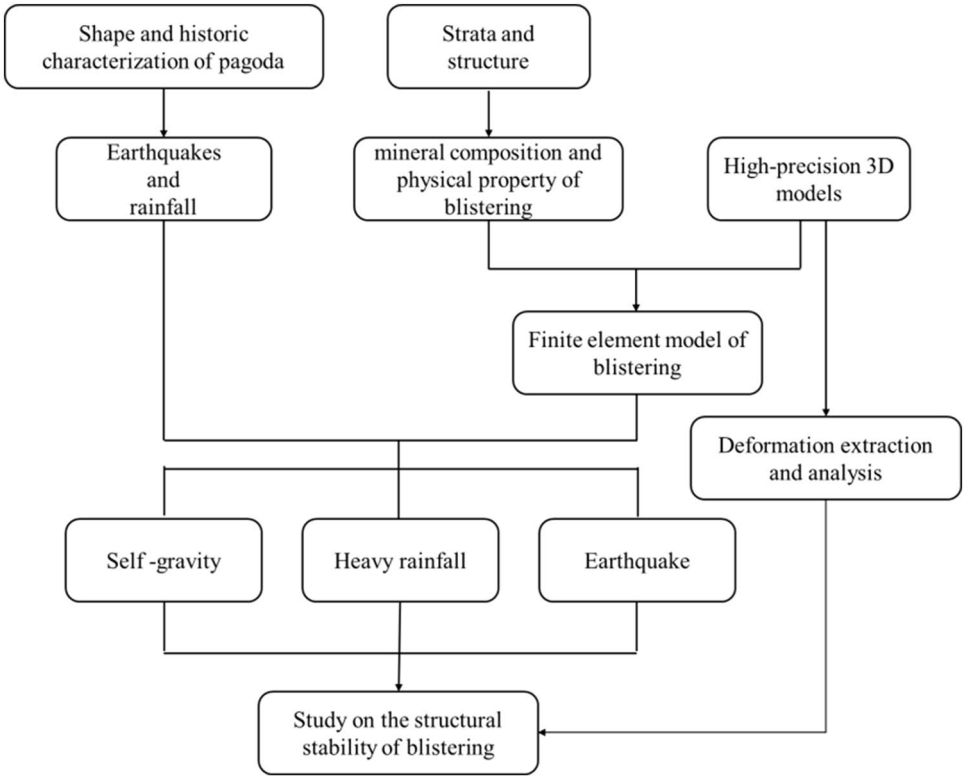

Fig. 1 Workflow diagram

the Qing Dynasty's 35th year of Kangxi due to an earthquake, resulting in structural instability. In that same year, the Vajrasana Pagoda underwent renovation to restore its original appearance, resulting in its current form (Fig. 2c).

Earthquake

Kunming Basin, formed during the Late Tertiary Period, lies on the western edge of the East Yunnan Fault Lake Basin. Its east and west borders are marked by the Pudu River fault zone and the Shuangqiao fault passage. The Vajrasana Pagoda is situated on the eastern branch of the Shuangqiao Fault Zone in Guandu District. According to the "History of the Five Elements of the Song Dynasty," Kunming's earliest recorded earthquake took place on December 21, 1302. To date, the region has experienced 27 earthquakes with a magnitude of 5 or higher [27] and 7 destructive earthquakes [28]. In the thirty-fifth year of Kangxi during the Qing Dynasty (1696 AD), an earthquake struck Kunming with an epicenter intensity of VII or higher, and a magnitude of 5.75 or more in the Guandu district [29]. This event caused the collapse of two small towers of the Vajrasana Pagoda, consistent with inscriptions on the stone. The other two towers also sustained significant damage. Furthermore, in the thirteenth year of Daoguang during the Qing Dynasty, a major earthquake with an epicenter VIII, located 40 km east of Kunming, resulted in the cracking of the east tower near the Vajrasana Pagoda and the fall of the west tower. According to the "Code for Earthquake Design of Buildings," the earthquake fortification intensity in Guandu District is 8 degrees (with an acceleration of 0.2 g), categorizing it as a seismically unstable area with a risk of earthquake damage.

Rainfall

Kunming belongs to the subtropical monsoon climate and annual precipitation is about 955 mm. The main flood season is from May to September, and its precipitation accounts for more than 40% of the annual precipitation. The World Meteorological Organization defined the heavy rain days (R20), particularly heavy precipitation (R95pTOT) and extreme precipitation (R99pTOT), to illustrate the regional extreme precipitation situation. From 1951 to 2016, the R20 was 24 days, R95pTOT was 700 mm, and R99pTOT was 325 mm [30]. There is a possibility of sudden heavy rainfall in this area. According to the statistics of regional precipitation from January 2017 to October 2022 (Fig. 3), rainfall is concentrated and large, with a maximum rainfall of 114.81mm in a single

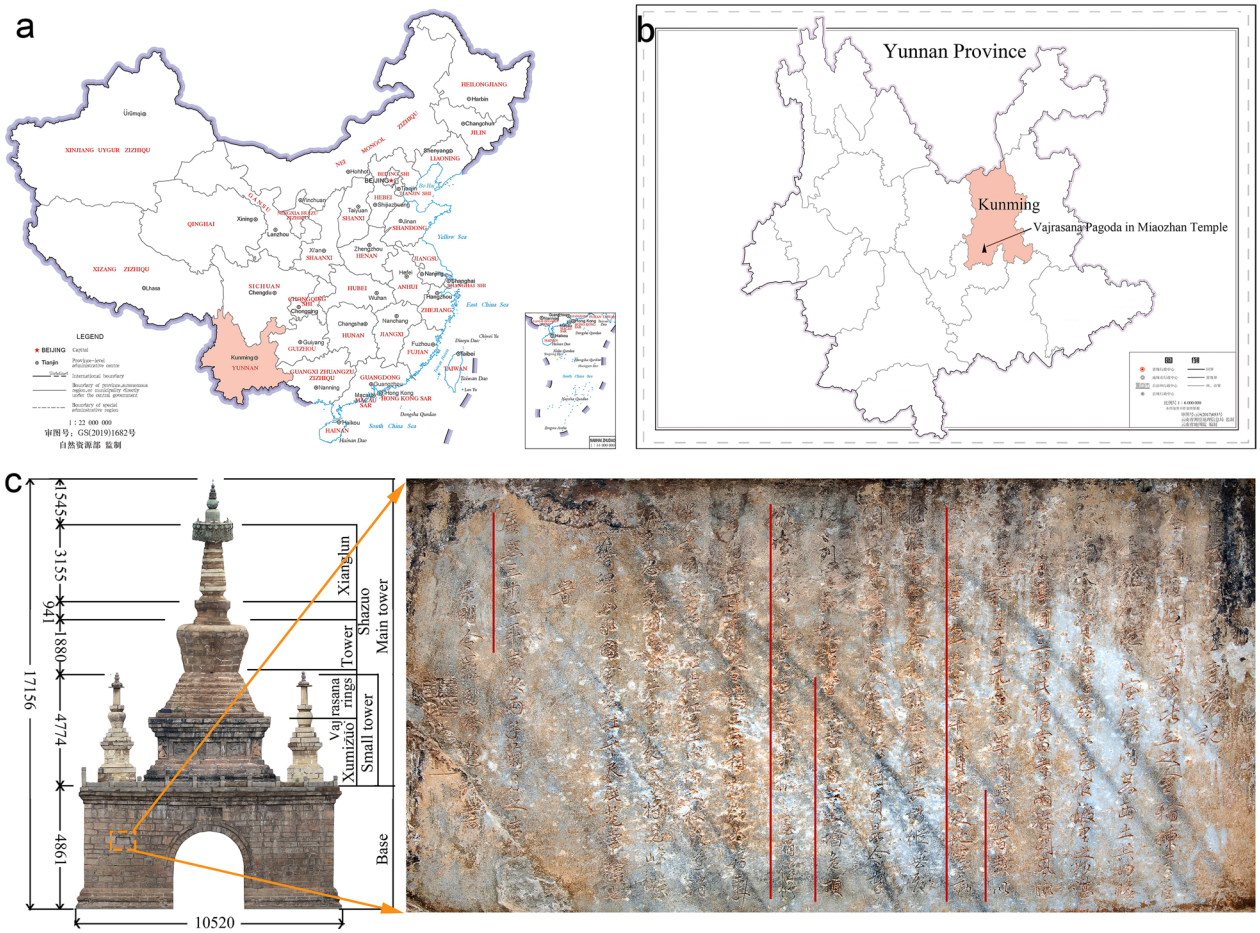

Fig. 2 **a** Location of Yunnan Province in China; **b** location of the Vajrasana pagoda in Miaozhan Temple in Kunming; and **c** exterior view and inscription of the "Reconstruction of the pagoda of Miaozhan Temple"

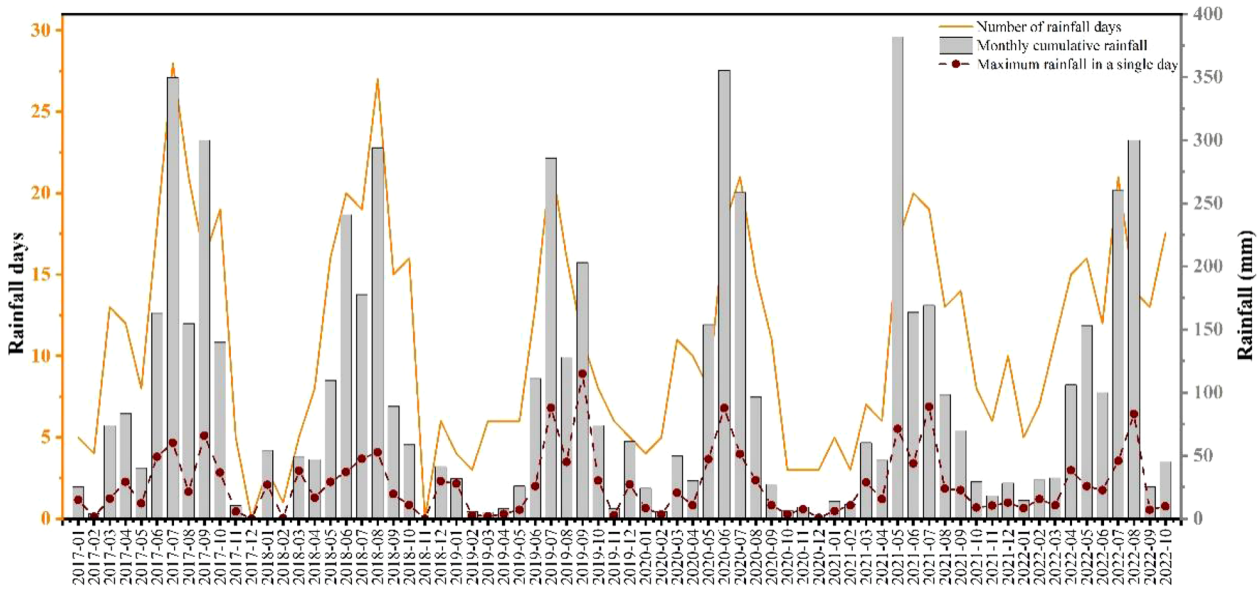

Fig. 3 Rainfall statistics of Guandu District from 2017 to 2022

day and a maximum of 28 days of cumulative rainfall per month. The cumulative monthly rainfall in June 2021 reached 382.02 mm. In the numerical study of rainfall states, the water-saturated state of the rock was studied using the saturated gravity of the rock.

Strata

This area is composed of an artificial accumulation (Q_4^{ml}) layer of the Quaternary period. The shallow part is the alluvial and lake sediment (Q_4^{al+l})and the strata consist of a snail shell layer, peat soil, and silty clay. The middle and the lower parts are alluvial and lake sediment (Q_4^{al+l}), and the strata consist of silt, peat soil, and clay.

Foundation

The Vajrasana Pagoda's foundation at Miaozhan Temple, estimated at 1350 tons, was constructed using dense piling. It employed fir and pine stakes with diameters ranging from 15 to 35 mm, spaced 200 mm apart. At the foundation's top, a mixture of lime, clay soil, and crushed snail shells was applied.

Methods and material

Methods

3D laser scanning

The 3D laser scanning equipment used is the Artec Space Spider by Artec 3D, with a scanning accuracy of 0.05mm and a speed of 7.5 frames per second. Data alignment occurs in real-time during scanning, aided by high-frequency LED lights that minimize the impact of natural light on accuracy.

The stone carvings on the main tower, measuring approximately 900 mm in length and 600 mm in height, were scanned from a distance of 20–30 cm to ensure precise collection. The scanning equipment maintained a vertical orientation to guarantee uniform point cloud quality, and complex areas were scanned multiple times for data completeness. The original point cloud data were denoised through redundancy removal, resulting in a uniform density and complete shape. This data was further processed by encapsulating it into a Triangulated Irregular Network (TIN) to repair any gaps and create a seamless grid surface.

To assess the blistering deformation of the Vajrasana Pagoda, laser scanning tests were conducted twice, following the same data acquisition method on April 23, 2020 (Phase 1) and January 24, 2021 (Phase 2).

Thin section identification test

The Leica DM 2700 polarizing microscope was used for the mineral analysis of stone. The stone sample was made into 35 mm × 25 mm × 0.03 mm thin slices, and the was observed at single polarization and orthogonal polarization condition. Using crystal optics and petrology, the mineral composition, structure, alteration, and metamorphism characteristics of the stones were determined.

X-ray diffraction test

A small amount of stone power was compressed and analyzed with Rigaku D/max 2200 X-ray diffractometer with Cu-K_a radiation, operating at 40 kV and 40 mA. The divergence slit, anti-scatter slit, and receive slit are 1° respectively.

Uniaxial compression strength test

The GCTS RTX-1000 equipment was used to determine the uniaxial compressive strength of sandstone. The dimension of the specimens is 50 mm in diameter and 100 mm in height.

FEM numerical simulation

To analyze the stress and strain of blistering, a three-dimensional finite element numerical modeling was carried out by ABAQUS software.

Material

The appearance and weathering of stones on the entire tower are consistent. Three samples were collected based on the structure: JGT-1 (base), JGT-2 (main tower), and JGT-3 (small tower). Stone types and composition were determined through thin section and X-ray diffraction tests. The mortar joint (JGT-4) from the base was also analyzed using X-ray diffraction.

Thin section identification (Fig. 4) revealed that the Vajrasana Pagoda stone at Miaozhan Temple is fine-grained quartz sandstone. X-ray diffraction spectrogram (Fig. 5) confirmed that the base, main tower, and small tower consist of the same materials, including quartz, calcite, and orthoclase. The mortar joint primarily contains quartz, calcite, albite, and orthoclase.

Laboratory uniaxial compression strength tests were performed to determine the compressive strength of the sandstone samples. Using stress–strain curves and uniaxial compressive test data, the cut-line modulus was used to calculate the modulus of elasticity according to the double-exponential classification principle for rocks. The average uniaxial compressive strength was 30.2 MPa (cov = 19.2%), and Young's modulus was 35.655 GPa (cov = 12.6%).

3D laser scanning and analysis

Point cloud model establishment

The study focused on the blistering area on the south side of the main tower of the Vajrasana Pagoda (Fig. 6). The

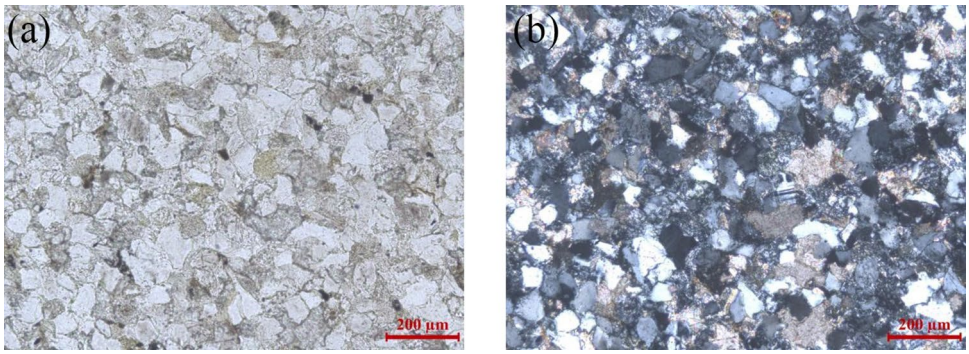

Fig. 4 Thin section identification of sandstone: **a** Single polarization; **b** orthogonal polarization

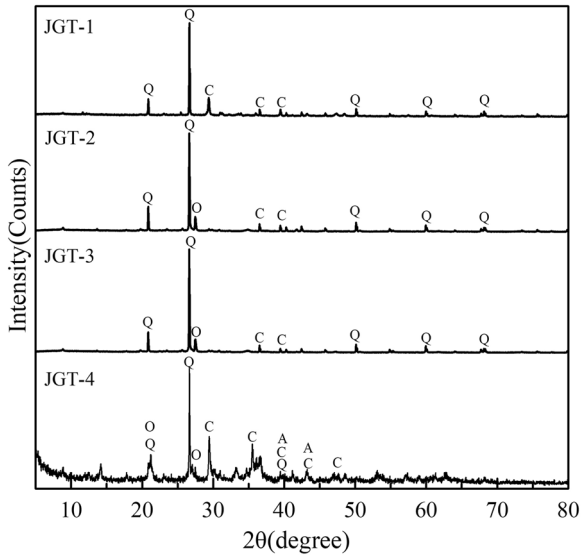

Fig. 5 X-ray diffraction spectra of samples (A: Albite,C: Calcite,O: Orthoclase,Q: Quartz)

blistering measures 861.51 mm in length and 525.62 mm in height.

The accuracy of the finite element analysis results is significantly influenced by the quality of the 3D laser scanning model. Therefore, a high-precision 3D point cloud model was employed for blistering modeling, with a point spacing finer than 0.204 mm (Fig. 7). After point cloud encapsulation, mesh repair, and precise surface processing, an IGS format NURBS surface was generated for mechanical calculations in ABAQUS software. This 3D model, based on the point cloud model, predominantly consisted of sandstone (Fig. 8). The material property parameters of the Vajrasana Pagoda are listed in Table 1.

In the finite element model, the negative Y-axis direction represents gravity, and the entire model is tetrahedrally meshed using the C3D10 element type. The model comprises 52,194 elements and 76,289 nodes after meshing.

Point cloud data comparison

The high-precision point cloud model of Phase 1 was the reference model, and the Phase 2 data was the comparison model. 5 feature points were selected from each model to calculate the corresponding space parameters, and to perform coarse registration. The average standard deviation of coarse registration was 0.58 mm (Table 2).

The iterative closest point (ICP) algorithm was used to build high-precision registration model [32] using the sum of squares of the residuals as the objective function. The coordinates of the comparison data were included in

Fig. 6 Blistering on the south side of the main tower

Fig. 7 **a** Orthographic image; **b** point cloud model; **c** triangulated irregular network

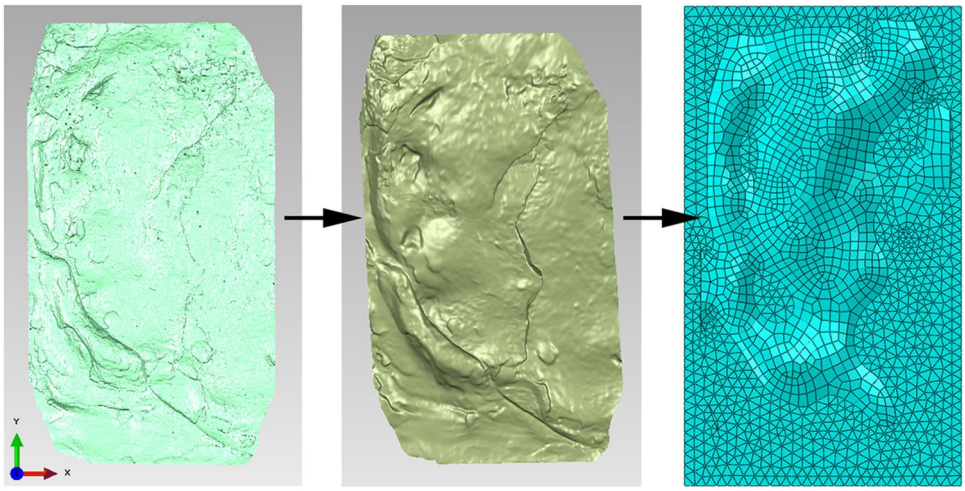

Fig. 8 FEM model of blistering

Table 1 Material properties of the Vajrasana pagoda in Miaozhan Temple [31]

Mechanical parameters	Density (kg/m^3)	Elastic modulus (MPa)	Poisson ratio	Depth (m)
The sandstone of the Vajrasana pagoda	2280	3.5e4	0.25	17.16
Foam mortar material of the underground space	800	2.4e4	0.35	4.7
Quaternary artificial accumulation (Q^{ml}) layer	1840	3.96e2	0.4	4
Quaternary alluvial lake (Q_4^{al+l}) layer	2000	4e2	0.4	7
Quaternary alluvial lake (Q_4^{al+l}) layer	2000	8.31e2	0.35	7.2
Bedrock	2800	1.0e6	0.2	1.8

the reference coordinate datum. With iteration tolerance set to 0.001mm, the convergence requirements were met after 11 iterations. A 3D color deviation model was generated after the registration.

Deformation extraction and analysis

The 3D color deviation model visually represents overall deformation characteristics and deformation trends through color deviations. Positive values indicate blistering expansion, while negative values indicate blistering detachment, with deformation depth correlating with the amplitude of change. In Fig. 9, the left and center regions of the blistering have detached by 0.95 mm, while the bottom area and right border have elevated. Non-blistered areas remain unchanged. Representative positions were selected to quantify the deformation, as illustrated in Fig. 10 and Table 3, all falling within the finite element analysis range.

Blistering is influenced by factors such as cultural relic materials, rainwater dissolution, dry–wet cycles, water-salt transport, crystallization, and temperature fluctuations. In the case of the Vajrasana Pagoda at Miaozhan Temple, temperature change plays a central role. Temperature disparities inside and outside the stone, mismatch of expansion/contraction coefficients, stone material heterogeneity, layered structure, and expansive clay minerals

contribute to blistering. The primary stone components, quartz and calcite, exhibit significantly different linear expansion coefficients. Additionally, the expansion coefficient of a mineral can change with crystallization direction, creating internal stress adjustments leading to both the expansion of existing blistering and the formation of new ones. The severity of erosion due to temperature differences primarily depends on the speed and magnitude of temperature changes, with more significant temperature fluctuations leading to more pronounced blistering development.

Numerical simulation analysis

Analysis in the self-gravity stress state

To study the stress and strain of blistering of Vajrasana pagoda, the FEM was used to investigate the stability of blistering. According to the fourth strength theory, the Mises stress represents the maximum stress on the unit. When the force exceeds the plastic strength, the rock will undergo irreversible deformation. Thus, Mises stress is taken as the stress of destruction. In the self-gravity stress state, as Fig. 11 shown, the Mises stress field distribution shows that the maximum stress of the upper part of the blistering is 13.98 Pa, and the stress values of the lower and left sides of the blistering are between 3.770 and 7.260 Pa. The distribution of the strain field shows that the maximum vertical strain of the blistering in the natural state is the upper part of the blistering, which is between 3.070×10^{-8} and 8.697×10^{-8}. The tensile strength of sandstone is about 2 MPa, so the stresses in various parts of the blistering are much smaller than the strength of the material. The analysis of the displacement field shows negligible blistering uplift on the order microns. In general, in the state of self-gravity stress state, the blistering of stone is stable.

Analysis in the heavy rainfall state

During heavy rainfall, the stone material is weakened. Figure 12 shows that the displacement fields of the material in the heavy rainfall state. The Mises stress field shows that the maximum stress of the blistering in the saturated state is 15.66 Pa. The strain field distribution shows that the maximum vertical strain occurs at the upper part of the blistering, which is about 1.218×10^{-7}. The stress of the blistering is much smaller than the strength of the material. The displacement field distribution shows only small displacement change at the bulge of the blistering

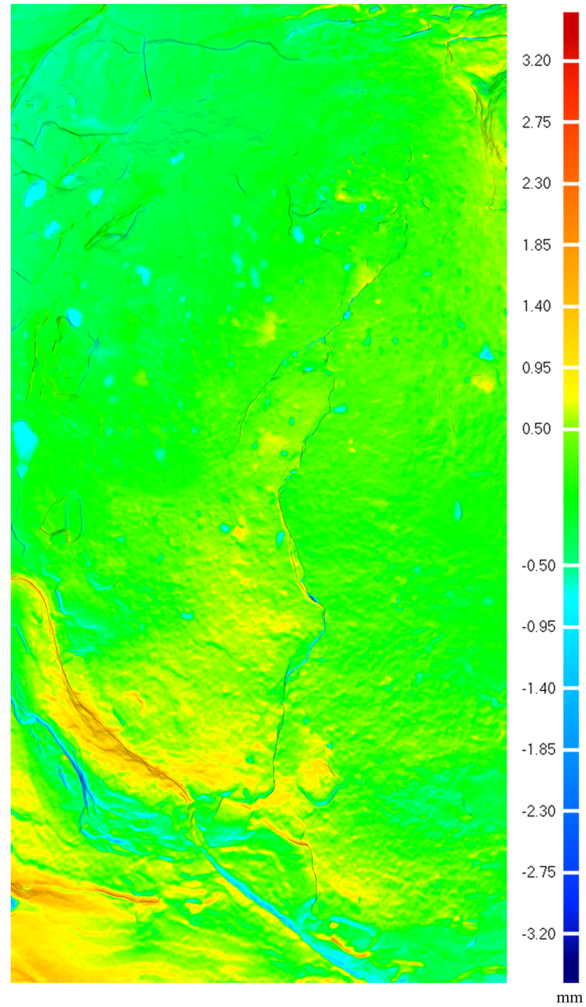

Fig. 9 3D color deviation model plot

Table 2 Coarse registration accuracy

Points	Phases 1(mm)			Phases 2(mm)			Deviation (mm)			
	Reference X	Reference Y	Reference Z	Comparison X	Comparison Y	Comparison Z	ΔX	ΔY	ΔZ	Deviation
A001	−138.14	163.30	47.53	−138.42	163.22	47.67	−0.28	−0.08	0.14	0.33
A002	−388.90	45.31	19.55	−388.26	44.90	19.75	0.65	−0.41	0.20	0.79
A003	56.38	−319.27	−69.49	56.62	−319.00	−69.96	0.24	0.28	−0.47	0.59
A004	381.21	−88.96	−22.35	381.57	−88.59	−22.56	0.36	0.37	−0.21	0.55
A005	288.68	173.27	34.74	289.30	173.43	34.62	0.63	0.16	−0.13	0.66

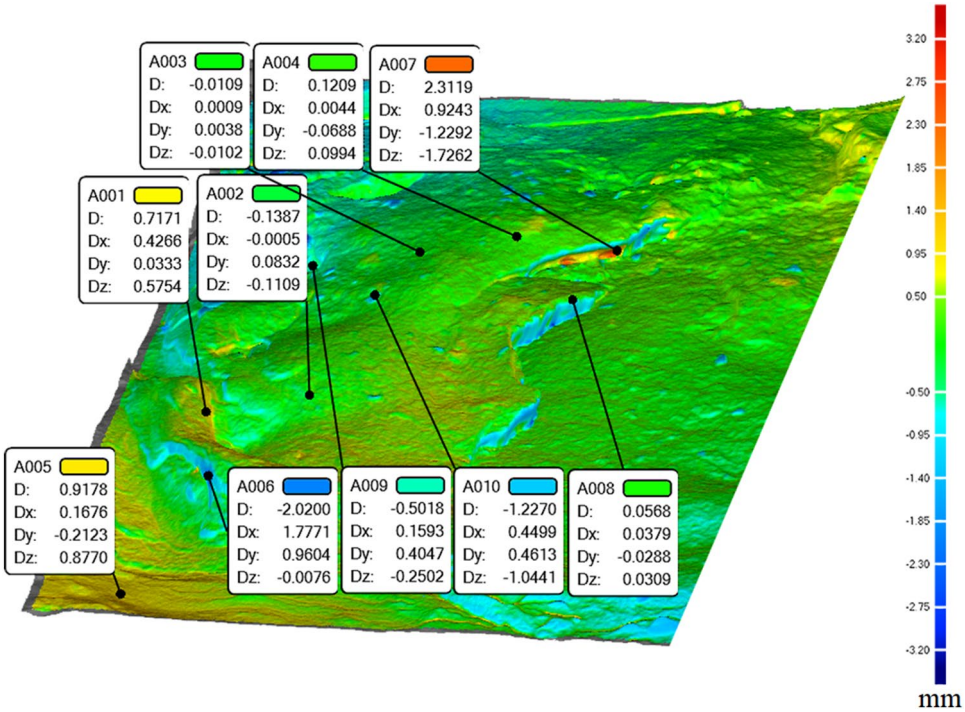

Fig. 10 Transverse plane of 3D color deviation model plot

Table 3 Data comparisons for different phases

Points	Deviation (mm)	ΔX (mm)	ΔY (mm)	ΔZ (mm)
A001	0.72	0.43	0.03	0.58
A002	−0.14	0.00	0.08	−0.11
A003	−0.01	0.00	0.00	−0.01
A004	0.12	0.00	−0.07	0.10
A005	0.92	0.17	−0.21	0.88
A006	−2.02	1.78	0.96	−0.01
A007	2.31	0.92	−1.23	−1.73
A008	0.01	0.04	−0.03	0.03
A009	−0.501	0.16	0.41	−0.25
A010	−1.23	0.45	0.46	−1.04

up to 0.01 mm. In general, the blistering of stone is stable during heavy rainfall.

Analysis in the earthquake state

In the earthquake state, as Fig. 13 shown, the material is in a saturated state. The Mises stress field distribution shows that the maximum stress of the upper part of the blistering is 8.69 Pa, and the stress of the other connections between the blistering and the body is from 4.14 Pa to 8.69 Pa. The strain field distribution shows that the maximum vertical strain is at the upper part of the blistering, about 1.697×10^{-7}. The distribution of the acceleration field shows that the maximum acceleration is at the blistering part connecting body, which is 0.76 m/s^2. The displacement field distribution large displacement 1.167 mm on the uplift part of the blistering under earthquake load, which could lead to breakage. Based on the above analysis, the upper part of the blistering may be broken in the earthquake state.

Conclusions

This study utilized 3D laser scanning technology to create a high-precision model and measured the physical and mechanical properties through XRD and thin section analysis. A 3D finite element model of the blistering was established, and the structural stability of the stone blistering of the Vajrasana Pagoda in Miaozhan Temple was analyzed under three different conditions. The key findings are as follows:

1. In the self-gravity stress state, the blistering remains safe, with stress levels below sandstone strength and minimal displacement.

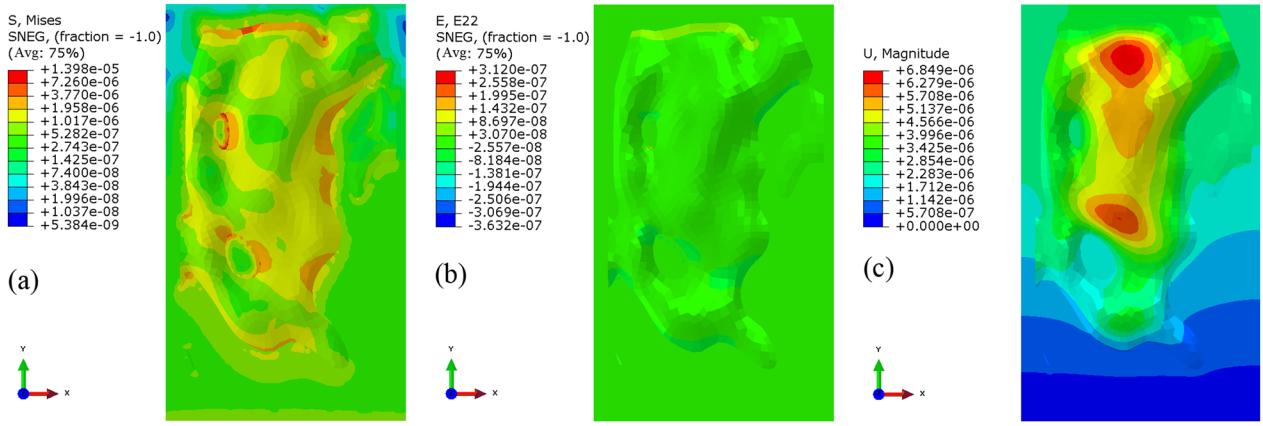

Fig. 11 Numerical simulation of the blistering in the self-gravity state. **a** mises stress values cloud map; **b** compressive strain values cloud map; **c** displacement values cloud map

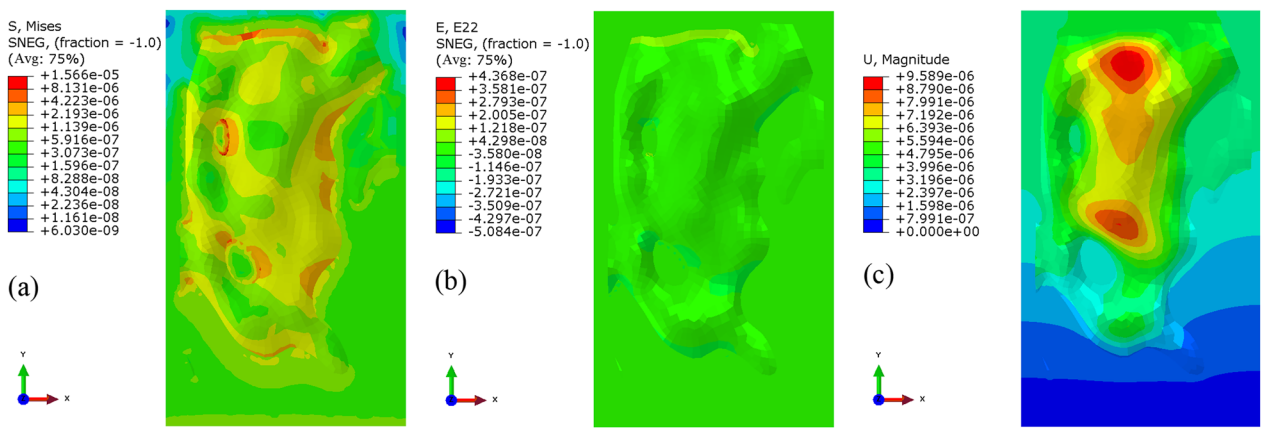

Fig. 12 Numerical simulation of the blistering in the heavy rainfall state. **a** mises stress values cloud map; **b** compressive strain values cloud map; **c** displacement values cloud map

2. Under heavy rainfall, the saturated sandstone in the blistering also exhibits safe conditions, with stress well below the material's strength and negligible displacement.
3. In an earthquake state, the blistering experiences stress close to its tensile strength. The risk is highest at the upper part junction with the side body, where the displacement can reach 1.167 mm.
4. The deformation analysis of the high-precision model from April 23, 2020 to January 24, 2021 showed that the left side of the blistering was detached, and the right edge and bottom area were raised. There was no deformation in the non-blistering area. The deformation area coincides with the FEM analysis.

These findings underscore the need for protective measures against potential earthquakes, such as shock protection, structural reinforcement, deformation monitoring, and other protective steps for the Vajrasana Pagoda in Miaozhan Temple. The study also lays the groundwork for stress–strain simulations of fragile, small-volume stone cultural relics with fine structures. Due to the blistering's fragile structure, contact methods for measuring physical and mechanical characteristics may not be suitable. While this study

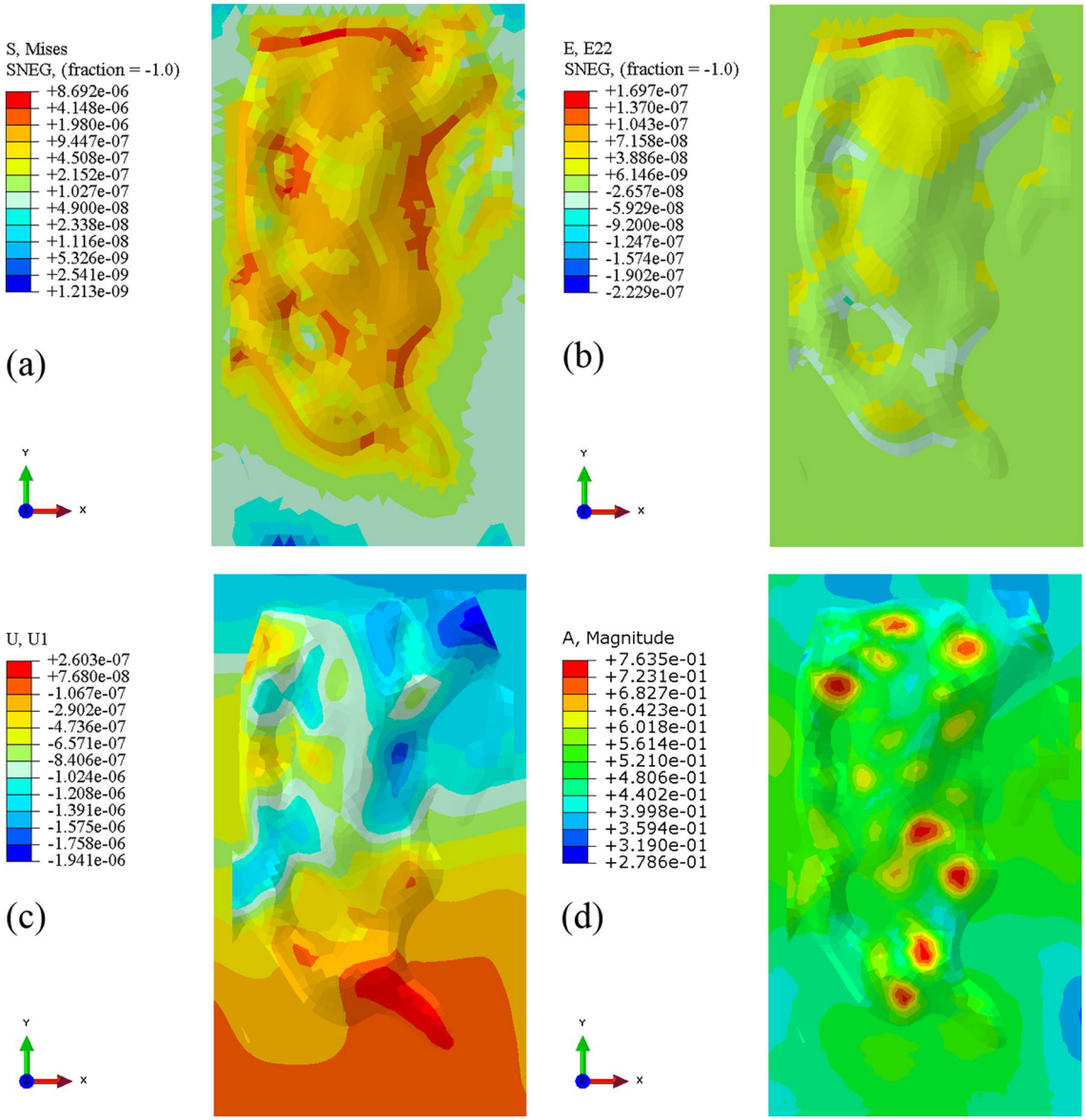

Fig. 13 Numerical simulation of the blistering in the earthquake state. **a** mises stress values cloud map; **b** compressive strain values cloud map; **c** displacement values cloud map; **d** acceleration cloud map

uses 3D laser scanning and FEM without cross-verification from other methods, ongoing sustainable monitoring is advisable.

Acknowledgements
The authors would like to express their great gratitude to Kunming Guandu District Museum, Beijing Guo Wenyan Cultural Relics Protection and Development Co., Ltd., China, University of Geosciences (Wuhan), and University of Science and Technology Beijing. This research was financially supported by the study on the protection of the Vajrasana pagoda in Miaozhan Temple.

Author contributions
HG provided support and guidance for this study. BL, YZ, XB, and YW performed an analysis and drafted the manuscript. YZ provided the samples and assistance in the study. DC made revisions to the paper. All authors read and approved the final manuscript.

Funding
The research was financially supported by the National Key R&D Program of China (grant number 2020YFC1522404) and the study on the protection of the Vajrasana pagoda in Miaozhan Temple.

Availability of data and materials
The datasets used during this study are available from the corresponding author upon request.

Declarations

Competing interests
The authors declare that they have no competing interests.

Received: 16 February 2023 Accepted: 8 November 2023
Published online: 04 December 2023

References

1. Centre for Research on the Epidemiology of Disasters (CRED). UNISDR-CRED Economic losses, poverty & disasters: 1998–2017 United Nations Office for Disaster Risk Reduction (UNISDR), Centre for Research on the Epidemiology of Disasters (CRED). Geneva: Centre for Research on the Epidemiology of Disasters (CRED); 2018.
2. Mateus L, Fernandez JG, Ferreira V, Pernao J, Mateus L, et al. Terrestrial laser scanning and digital photogrammetry for heritage conservation: Case study of the Historical Walls of Lagos, Portugal. Int Arch Photogramm Remote Sens Spatial Inf Sci. 2019;42:843–7. https://doi.org/10.5194/isprs-archives-XLII-2-W11-843-201.
3. Costamagna Erik C, Mario SQ, Nicoletta B, Nuno M, Paulo BL, Su S, Yin MP, Aungzaw ME, et al. Advanced non-destructive techniques for the diagnosis of historic buildings: the Loka-Hteik-Pan temple in Bagan. J Cult Herit. 2020;43:108–17. https://doi.org/10.1016/j.culher.2019.09.006.
4. Sigurdardottir DH, Glisic B. On-site validation of fiber-optic methods for structural health monitoring: streicker Bridge. J Civ Struct Heal Monit. 2015;5:529–49. https://doi.org/10.1007/s13349-015-0123-x.
5. Hemeda S. Geotechnical modelling of the climate change impact on world heritage properties in Alexandria. Egypt Herit Sci. 2021;9(1):73. https://doi.org/10.1186/s40494-021-00547-8.
6. Hemeda S. 3D finite element coupled analysis model for geotechnical and complex structural problems of historic masonry structures: conservation of Abu Serga church, Cairo. Egypt Herit Sci. 2019;7(1):1–19. https://doi.org/10.1186/s40494-019-0248-z.
7. Endo Y, Llorens MS, Roca P, Pelà L. Dynamic identification and static loading tests of timbrel vaults: application to a Modernist 20th century heritage structure. Int J Archit Herit. 2017;11(4):607–20. https://doi.org/10.1080/15583058.2016.1277566.
8. Malcata M, Ponte M, Tiberti S, Bento R, Milani G. Failure analysis of a Portuguese cultural heritage masterpiece: Bonet building in Sintra. Eng Fail Anal. 2020;115: 104636. https://doi.org/10.1016/j.engfailanal.2020.104636.
9. Zhao SJ, Yang YQ, Dai JW. Study on dynamic characteristics and seismic response of Yuhua Pavilion in the Forbidden City. World Earthquake Eng. 2020;36(1):85–92 (**in Chinese**).
10. Chen F, Xu H, Zhou W, Zheng W, Deng Y, Parcharidis I. Three-dimensional deformation monitoring and simulations for the preventive conservation of architectural heritage: a case study of the Angkor Wat Temple, Cambodia. Gisci Remote Sens. 2021;58(2):217–34. https://doi.org/10.1080/15481603.2020.1871188.
11. Fu CH, Shi YC. Research on dynamic damage characteristics of country rock of Mogao Grottoes under earthquake loading. Northwestern Seismol J. 2004;3:75–82.
12. Hemeda S. Geo-environmental monitoring and 3D finite elements stability analysis for site investigation of underground monuments. Horemheb tomb (KV57), Luxor, Egypt. Herit Sci. 2021;9(1):17. https://doi.org/10.1186/s40494-021-00487-3.
13. Buchta D, Heinemann C, Pedrini G, Krekel C, Osten W. Combination of FEM simulations and shearography for defect detection on artwork. Strain. 2018;54(3): e12269. https://doi.org/10.1111/str.12269.
14. Balletti C, Beltrame C, Costa E, Guerra F, Vernier P. 3D reconstruction of marble shipwreck cargoes based on underwater multi-image photogrammetry. Digital Appl Archaeol Cult Herit. 2016;3(1):1–8. https://doi.org/10.1016/j.daach.2015.11.003.
15. Zakaria A M, Said A M. 3D reconstruction of a scene from multiple uncalibrated images using close range photogrammetry. IEEE; 2010. p.1–5. https://doi.org/10.1109/ITSIM.2010.5561358.
16. Remondino F, Rizzi A, Barazzetti L, Scaioni M, Fassi F, Brumana R, Pelagotti A. Review of geometric and radiometric analyses of paintings. Photogram Rec. 2011;26(136):439–61. https://doi.org/10.1111/j.1477-9730.2011.00664.x.
17. Della TS. Italian perspective on the planned preventive conservation of architectural heritage. Front Arch Res. 2021;10(1):108–16. https://doi.org/10.1016/j.foar.2020.07.008.
18. Andrés AN, Pozuelo FB, Marimón JR, de Mesa GA. Generation of virtual models of cultural heritage. J Cult Herit. 2012;13(1):103–6. https://doi.org/10.1016/j.culher.2011.06.004.
19. Bouziani M, Chaaba H, Ettarid M. Evaluation of 3D building model using terrestrial laser scanning and drone photogrammetry. Int Arch Photogramm Remote Sens Spat Inf Sci. 2021;46:39–42. https://doi.org/10.5194/isprs-archives-XLVI-4-W4-2021-39-2021.
20. Jo YH, Hong S. Three-dimensional digital documentation of cultural heritage site based on the convergence of terrestrial laser scanning and unmanned aerial vehicle photogrammetry. ISPRS Int J Geo-Inf. 2019;8(2):53. https://doi.org/10.3390/ijgi8020053.
21. Venuti V, et al. In situ diagnostic analysis of the XVIII century Madonna della Lettera panel painting (Messina, Italy). Spectrochim Acta Part A Mol Biomol Spectrosc. 2020;228: 117822. https://doi.org/10.1016/j.saa.2019.117822.
22. Zhang Q, Gao F, Zhang AW. Statistical Methods of Analysis Methods Based on a Combination of Mural Diseas. J Commun Univ China; 2013; 20(05):29–34+28.
23. Xia GF, Hu CM, Wang YM. Study on the true three-dimensional detection method of cultural relic surface disease. China Cult Herit Sci Res. 2018;01:89–96 (**in Chinese**).
24. Pieraccini M, Guidi G, Atzeni C. 3D digitizing of cultural heritage. J Cult Herit. 2001;2(1):63–70. https://doi.org/10.1016/S1296-2074(01)01108-6.
25. Dorji L. A Study on Guandu Varjar-seat Pagoda of Tibetan Buddhism in Kunming. J Tibet Univ Soc Sci. 2017;32(02):59–64.
26. Shao Z, Wu Y, Ji L, Diao F, Shi F, Li Y, Li X. Assessment of strong earthquake risk in the Chinese mainland from 2021 to 2030. Earthquake Res Adv. 2023;3(1): 100177. https://doi.org/10.1016/j.eqrea.2022.100177.
27. Sichuan, Yunnan and Tibet Seismological Bureau (Office), Compiled by the Earthquake Briefing Catalogue, Southwest Earthquake Briefing, Sichuan Science and Technology Press; 1988. **(in Chinese)**
28. Min ZQ. Seismic risk in Kunming area. J Seismol Res. 1989;02:97–102 (**in Chinese**).
29. Zhang Y, Romanelli F, Vaccari F, Peresan A, Jiang C, Wu Z, Panza GF. Seismic hazard maps based on Neo-deterministic Seismic Hazard Assessment for China Seismic Experimental Site and adjacent areas. Eng Geol. 2021;291: 106208. https://doi.org/10.1016/j.enggeo.2021.106208.
30. Wu L, Peng X, Ma Y, Cheng X, Gong H, Dong L. Variation characteristics of extreme temperature and precipitation events during 1951–2016 in Kunming. J Yunnan Univ Nat Sci Ed. 2019;41(1):91–104 (**in Chinese**).
31. Zhang Y, Feng XT, Zhang X, Wang Z, Sharifzadeh M, Yang C, Zhao J. Strain energy evolution characteristics and mechanisms of hard rocks under true triaxial compression. Eng Geol. 2019;260: 105222. https://doi.org/10.1016/j.enggeo.2019.105222.
32. Besl PJ, Mckay ND. Method for registration of 3-D shapes. IEEE Trans Pattern Anal Mach Intell. 1992;14(2):239–56. https://doi.org/10.1109/34.121791.

Publisher's Note